International Journal for Housing Science and Its Applications
Publish August 6, 2025. Volume 46, Issue 3 Pages 5598-5609

https://doi.org/10.70517/ijhsa463483

Simulation-based optimization of nanocarrier design for loaded anticancer drug adriamycin photothermal sustained release system and its drug release characteristics

Lili Deng[1,*] and Xue Zhou[1]
[1] Zhengzhou Technical College, Zhengzhou, Henan, 450121, China
Corresponding authors: (e-mail: zzybiodll@126.com).

Abstract Cancer has become the second largest “killer” threatening human life, and it is expected that by 2030, the number of deaths will exceed 13.1 million per year globally. Adriamycin, as a widely used anticancer drug in clinical practice, faces limitations such as dose-dependent cardiotoxicity and other side effects. In this study, two nanocarrier systems, D-PNAx nanogel and PGFMSN particles, were designed using a simulation-simulation optimization method, characterized by dynamic light scattering method, transmission electron microscopy, and X-ray powder diffraction, and evaluated for drug release properties, biocompatibility, and antitumor effects. The results showed that L-CS-g-PNIPAM nanoparticles had relatively high drug loading (13.6%) and encapsulation rate (75.2%), and the particle sizes were all below 350 nm (275.1±19.2 nm), which were suitable for targeting tumors via EPR effect. pH and temperature responsiveness studies showed that under the condition of the tumor microenvironment (pH 5.0,37°C), 72 hour cumulative drug release rate could reach 85%, which was significantly higher than normal physiological conditions. In vivo antitumor experiments confirmed the targeting and safety of the nanocarrier system. The copper ion content of lung and tumor tissues in the CuS-PEI-siRNA-SFNs group was significantly higher than that in the CuS group, while the hemolysis rate was only 0.1%, which was much lower than that in the CuS group (49.2%). In this study, we successfully constructed a photothermal slow-release nanocarrier system for adriamycin, which provides a new strategy to improve the effect of tumor treatment and reduce drug toxicity.

Index Terms Nanocarrier, Adriamycin, Photothermal therapy, Sustained-release system, Antitumor, Biocompatibility

I. Introduction

Cancer, also known as malignant tumors, has risen to become the second leading “killer” of humans after cardiovascular disease [1]. According to the World Health Organization (WHO), about 7.6 million people died of cancer worldwide in 2008, and it is expected that this number will continue to rise, and by 2030, it will exceed 13.1 million. While cancer poses a serious threat to patients' lives and causes them great suffering, it also imposes a heavy economic burden on patients' families and society [2]. Adriamycin is a widely used anticancer drug for clinical treatment, which belongs to a group of antibiotic-like chemicals with excellent antitumor activity and is widely used in the treatment of many types of cancer [3]. Like most antitumor drugs, adriamycin suffers from dose-dependent cardiotoxicity, which not only affects the quality of patient survival and limits the clinical application of adriamycin, but may also be accompanied by some side effects, such as nausea, vomiting, and bone marrow suppression [4], [5]. Therefore, liposomal adriamycin is gradually put into use, liposome wrapped chemotherapeutic drugs injected into the body, which can significantly slow down the clearance of the drug in the bloodstream and prolong the in vivo action time, in order to improve the effect of tumor suppression, but liposomal such agents release a large amount of energy in a short period of time, which leads to the sharp increase in blood concentration, and insufficient response of the tumor microenvironment [6]-[8]. In addition, the combination of drugs with different molecular targets can, on the one hand, increase the genetic barriers that need to be overcome for cancer cell mutation and delay the adaptive progression of cancer. On the other hand, the simultaneous action of chemotherapeutic drugs with different targets on cancer cells can synergistically improve the therapeutic effect of the drugs [9], [10]. However, current combination chemotherapy is far from perfect as designed. Different pharmacokinetic, biodistribution and transcellular membrane delivery properties make dose optimization of combination chemotherapy difficult [11]. The use of nanoscale drug carriers, to assist combination chemotherapy can somehow overcome these difficulties [12]. Therefore, the development of drugs with efficient tumor targeting, palliative release, and effective response in the microenvironment has become a sought-after goal.

Photothermal therapy (PTT) is an emerging noninvasive cancer treatment that relies on the use of photothermal transforming substances (PTAs) to absorb specific wavelengths of near-infrared light (NTR) and convert it into heat to destroy cancer cells [13]. Compared with traditional manual surgery, radiation or chemotherapy, PTT has more targeted and lower adverse side effects. With the development of nanotechnology, PTA has also achieved significant improvement [14], [15]. Meanwhile, since PTA is a key component in realizing PTT, its water solubility and biocompatibility, as well as photothermal conversion rate, have a significant impact on its efficacy [16]. In addition, PTT can be combined with other treatments such as chemotherapy, photodynamic therapy, gene therapy and immunotherapy to fight cancer. However, in clinical practice, the low match between the structural properties of the carrier and the analytical properties of adriamycin in the photothermal drug delivery system results in a poor slow-release effect, and some of the nanomaterials used in the carrier may cause other toxicities under long-term use [17]-[21]. Researchers need to actively explore new technical approaches to solve such problems.

Cancer, also known as malignant tumors, has risen to become the second leading “killer” of humans after cardiovascular disease. According to the World Health Organization (WHO), about 7.6 million people worldwide died of cancer in 2008, and it is expected that this number will continue to rise, and by 2030 it will exceed 13.1 million. Cancer poses a serious threat to patients' lives and causes them great pain, and at the same time, it also brings a heavy economic burden to patients' families and the society. Adriamycin is a widely used anticancer drug for clinical treatment. It belongs to a group of antibiotic-like chemicals with excellent antitumor activity and is widely used in the treatment of many types of cancer. Like most antitumor drugs, adriamycin suffers from dose-dependent cardiotoxicity, which not only affects the quality of patient survival and limits the clinical application of adriamycin, but may also be accompanied by side effects such as nausea, vomiting, and myelosuppression. Therefore, liposomal adriamycin is gradually put into use. Liposomes wrapped around chemotherapeutic drugs injected into the body can significantly slow down the clearance of the drug in the bloodstream and prolong the in vivo action time in order to improve the effect of tumor suppression, but liposomes of this type of agents release a large amount of energy in a short period of time, which leads to a sharp increase in blood concentration and insufficient response of the tumor microenvironment. In addition, the combination of drugs with different molecular targets can, on the one hand, increase the genetic barriers that need to be overcome for cancer cell mutation and delay the adaptive progression of cancer. On the other hand, the simultaneous action of chemotherapeutic drugs with different targets on cancer cells can synergistically improve the therapeutic effect of the drugs. However, current combination chemotherapy is far from perfect as designed. Different pharmacokinetic, biodistribution and transcellular membrane delivery properties make dose optimization of combination chemotherapy difficult. The use of nanoscale drug carriers to assist combination chemotherapy can, to some extent, overcome these challenges. Therefore, the development of drugs with efficient tumor targeting, palliative release, and effective response in the microenvironment has become a sought-after goal. Photothermal therapy is an emerging non-invasive cancer treatment that relies on the use of photothermal conversion substances to absorb specific wavelengths of near-infrared light and convert it into heat to destroy cancer cells. Compared with traditional manual surgery, radiation or chemotherapy, photothermal therapy is more targeted and has fewer adverse side effects. With the development of nanotechnology, photothermal conversion substances have also made significant improvements. At the same time, the water solubility, biocompatibility, and photothermal conversion rate of photothermal conversion substances, which are the key components for realizing photothermal therapy, have a significant impact on its efficacy. In addition, photothermal therapy can be combined with other therapeutic means such as chemotherapy, photodynamic therapy, gene therapy and immunotherapy to fight cancer. However, in clinical practice, the low match between the structural properties of the carrier and the analytical properties of adriamycin in photothermal drug delivery systems results in a poor slow-release effect, and some of the nanomaterials used in the carriers may cause other toxicities under long-term use.

In this study, two nanocarrier photothermal retardation systems for adriamycin-loaded nanocarriers, D-PNAx nanogels and PGFMSN particles, will be designed and prepared by the simulation and simulation optimization method. By characterizing their physicochemical properties, evaluating the drug release behavior, studying the biocompatibility and antitumor activity, the structure-property relationship of the nanocarriers will be systematically explored, which will provide a scientific basis for the construction of a highly efficient and safe photothermal chemotherapeutic combination therapy platform, and ultimately solve the various clinical problems existing in the traditional adriamycin dosage forms, and promote the development of antitumor drug delivery systems.

II. Adriamycin-induced assembly of D-PNAx nanogels

II. A.Materials and Instruments

The reagents and materials used in this section of the experiment are shown in Table 1.

Table 1: Reagents and materials

Reagent name	English name/abbreviation	Manufacturer	Level/specification
amycin	Dox·HCl	Beijing huaibo technology co., LTD	
DMEM medium	DMEM	Life Technologies	Biochemical reagent
Fetal cow serum	FBS	Thermo scientific	Biochemical reagent
Dimethyl sulfone	DMSO	National drug	Analytical purity
3-(4, 52-dimethythiazole -2) -25-diphenyl tetraazolbromide	MTT	Sigma-Aldrich	98 %
Methyl alcohol	Methonal	National drug	Analytical purity
Concentrated hydrochloric acid	HCl	National drug	Analytical purity
polyformaldehyde	PFA	Biosharp	≥99 %
Red cell cracking liquid		Azure sky	
HepG2 cells	Laboratory preservation		
H22 cell	Laboratory preservation		
Balb/C mice	male	Hubei disease prevention control center	

The list of instrument information used in the experiment is shown in Table 2.

Table 2: Instrument information

Instrument name	Type	Manufacturer
Electronic balance	BSA124S	Seidus science instrument co., LTD
Magnetometer pH meter	pHS-3E	Shanghai yielectric science instrument co., LTD
Electric thermostat	DHG type	Shanghai jinghong experimental equipment co., LTD
Ultraviolet visible spectrophotometer	TU-1901	Beijing general instrument co., LTD
Laser granulometer	Nano ZS90	malvern
Small animal living imaging system	IVIS Lumina XR	Caliper life sciences
Fluorescence spectrophotometer	FL4500	Hitachi
Transmission electron microscope	Tecnai G2 20	FEI
X-ray powder diffractometer	Empyrean	Panina, Netherlands
Inverted microscope	CKX31	Olympus Japan
Advanced rotary rheometer	Kinexus ultra+	Marvin
Double single surface cleaning table	SW-CJ-2FD	Suzhou purification equipment co., LTD
microplatereader	318C	Shanghai sanke instrument co., LTD
Carbon dioxide incubator	HERA cell 150	Thermo sicentific, Germany

II. B.Experimental Methods

II. B. 1) Assembly and drug loading of D-PNAx nanogels

A 10 mL solution of PNAx block polymer (pH 8.0, 5.0 mg/mL) with four degrees of hydrolysis was prepared and transferred to a dialysis bag with a molecular weight cutoff of 3800, and then the bag was immersed in 500 mLDox solution (100 μg/mL) with slow stirring, protected from light. The amount of Dox outside the dialysis bag was determined by fluorescence spectrophotometry (E_x =485 nm, E_m =554 nm), and the drug loading (DL) and encapsulation rate (EE) were calculated according to equations (1) and (2).

$$DL\% = \frac{W_0 - C_f V_f}{C_n V_n + (W_0 - C_f V_f)} \times 100\% \quad (1)$$

$$EE\% = \frac{W_0 - C_f V_f}{W_0} \times 100\% \quad (2)$$

where W_0 is the amount of Dox fed, C_f and V_f are the concentration and volume of free Dox in the whole system, and C_n and V_n are the concentration and volume of aqueous PNAx solution.

II. B. 2) Characterization of D-PNAx nanogels

(1) Determination of particle size and zeta potential of D-PNAx nanogels

Dynamic light scattering (DLS) was used to determine the particle size and zeta potential of D-PNAx nanogels. First, the D-PNAx nanogels were diluted to 1.0 mg/mL with ultrapure water, and then their hydrodynamic diameters and distributions as well as zeta potentials were determined. The instrumental parameters were He-Ne laser (λ=633 nm), 4 mW, with a scattering angle of 90°.

(2) Observation of D-PNAx nanogel morphology

The D-PNAx nanogel was dropped on a sealing film, adsorbed on a carbon film-covered copper mesh for 10 min, then transferred to filter paper for drying, and a drop of 2.0% phosphotungstic acid solution was added to the carbon film-covered copper mesh with the D-PNAx nanogel adsorbed after 5.0 min, and then the morphology and the size of the nanogel were determined by a transmission electron microscope after complete drying with an operating voltage of 200 kV.

(3) Crystallographic characterization of Dox in D-PNAx nanogel

The D-PNAx nanogel was rapidly frozen by liquid nitrogen and freeze-dried to obtain the freeze-dried powder of D-PNAx nanogel, and the crystallographic analysis was carried out by X-ray powder diffractometer, scanning angle: 10°~90°.

II. B. 3) Drug release studies with D-PNA100 nanogel dispersions

In order to better simulate the in situ drug release environment in the tumor, we designed an in vitro drug elution device suitable for hydrogel drug delivery system. The schematic diagram of the drug elution device is shown in Fig. 1, and the whole device was in a light-avoiding environment at 37 °C. The drug content was detected by fluorescence spectrophotometer, and the accumulated release (AR) was calculated by equation (3):

$$AR = \frac{\sum_{i=1}^{x} C_i V_i}{\sum_{i=1}^{n} C_i V_i} \times 100\% \tag{3}$$

where C_i and V_i represent the concentration of Dox in the i th beaker and the volume of the solution, respectively.

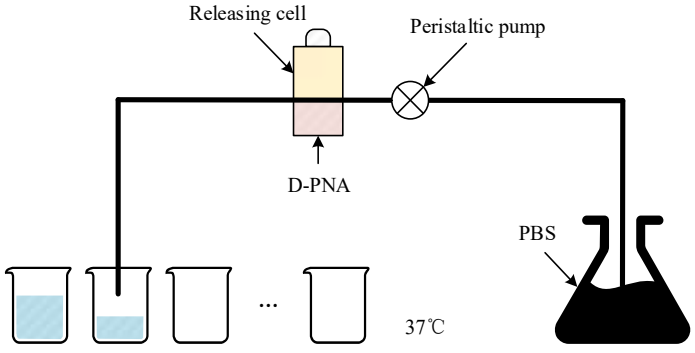

Figure 1: Schematic diagram of the drug elution device

II. B. 4) Temperature-sensitive sol-gel phase transition studies

D-PNAx nanogel dispersions with concentrations of 4%-10% (w/v) and 2 mL of the corresponding PNAx polymer solution were prepared, and the pH of the PNAx was adjusted with an appropriate amount of 1.0 molL NaOH. The dynamic viscoelasticity of the D-PNAx dispersion was determined using the stress constant mode of the advanced rotational rheometer. Instrument parameters: PP50 plate, 50 mm diameter, 0.5 mm gap, 0.05 Pa pressure, temperature range 20 ℃~50 ℃, temperature increase rate 1.0 ℃/min, frequency 1.0 Hz.

II. B. 5) Biocompatibility and cytotoxicity evaluation

Cytotoxicity assay was performed using HepG2 cells for MTT assay.After HepG2 cells were cultured to the logarithmic growth phase, the cells were digested and collected, and the cells were diluted to 1×105 cells/mL.The

HepG2 cells were spread in a 96-well plate at 5×103 cells per well, and the cells were cultured in the plate for 24 h. After the cells were cultured for 24 h in the plate, the medium was aspirated, and PNA100 was diluted with DMEM medium to 2- 0 μg/mL, 20 μg/mL, 100 μg/mL, 200 μg/mL, and free Dox and D-PNA100 nanogels were diluted to 0.1 μgnL, 1.0 μg/nL, 5.0 μg/nL, 10 μg/nL, respectively, and then co-incubated with HepG2 cells for 24 h and 48 h. DMEM medium containing cells was used as a negative control. DMEM medium was used as blank control. After adding 20 μL of 5.0 mg/mL MTT, the cells were incubated in the incubator for 4 h. After removing the culture medium, 150 μLDMSO was added to dissolve the metazan, and the absorption value of metazan at 492 nm was detected by an enzyme marker [22]. Cell survival was calculated according to formula (4):

$$Cellviability = \frac{OD_s - OD_b}{OD_n - OD_b} \times 100\% \quad (4)$$

where OD_s, OD_b and OD_n represent the OD values of the sample, the blank and the negative control, respectively.

II. B. 6) Evaluation of in vivo anti-tumor activity

Tumor-bearing mice were used as an animal model for pharmacodynamic evaluation. 100 μL of H22 tumor cell suspension (2.0 × 107 cells/mL) was injected into the subcutaneous tissues of the right hind leg of mice, and the tumor grew to 150-200 mm³ after 8-10 days. tumor-bearing mice were randomly divided into four groups of five mice each, and 50 μL of saline, PNA100 polymer dispersion (100 mg/mL), Dox, and D-PNA100 nanogel dispersion (17.5 mg/kg in the last two groups) were injected intratumorally, and Dox was dosed at 17.5 mg/kg every day after the injection. (100 mg/mL), Dox and D-PNA100 nanogel dispersion, in which the dose of Dox in the latter two groups was 17.5 mg/kg. The mice were weighed every day after the injection, and the length and width of the tumors were measured, and the tumor volume v was calculated as $v = LW^2/2$ (L and W are the length and width of the tumor, respectively) , and the survival rate was recorded [23].

II. B. 7) In vivo Dox distribution studies

H22 hormonal Balb/C mice were used as a model to study the drug retention behavior in the tumor. When the tumors of mice grew to about 200 mm³, 50 μLD-PNA100 nanogel dispersion with free Dox solution was injected into the tumor, and the mice were dislocated and executed by cervical dislocation on the first (1h, 1, 3, 7, and 10 days), respectively, and the tissues of the tumor, heart, liver, spleen, lungs, and kidneys were taken out, placed on the black adhesive plate and arranged, and placed on the small animal imaging system for scanning. The scanning parameters were set as follows: exposure time was 0.5 s, binning value was 1, and shutter (f/stop) was 2.

The tumors were weighed and ground with ultrapure water (0.2g/0.5mL), and after grinding, 2 times volume of methanol and hydrochloric acid mixture (v/v=94:6) was added for zero extraction, and then vortexed by vortexing instrument for 5min, and then left to stand for 30min away from light, and finally centrifuged at 10,000rpm for 15min, and the supernatant was taken and stored in the refrigerator at 4℃. The content of Dox in the tissues was detected by fluorescence spectrophotometer, E_x =488nm, E_m =554nm, and the width of slit was 10nm.

The establishment of tissue standard curve: take the blank tumor of mouse H22, grind it with ultrapure water (0.2g/0.5mL), add free Dox after grinding, extract it with a mixture of methanol and hydrochloric acid, centrifuge and take the supernatant, and the concentration range of Dox was head 0.1μg~1.0μg/mL.

III. 3. Methods of preparation of adriamycin

III. A. Synthesis of MSN-FA@Gelatin-PEG (PGFMSN) particles

Dissolve 1.00 g of CTAB in 480 mL of deionized water, add 3-5 mL of 2 molL-1 NaOH solution, mix well and then warm the mixed solution to 80 °C. 5.00 mLTEOS was added dropwise to the mixed solution and stirred for 2 h to obtain a white precipitate. The solid product was separated by high-speed centrifugation, and washed with deionized water and ethanol for three times sequentially. In order to remove the template CTAB, after discarding the supernatant, the sample was dispersed in 80mL of anhydrous ethanol, and 0.80mL of concentrated HCl was added, and stirred and refluxed at 80C for 16 h. The product was separated by high-speed centrifugation, and washed three times each with anhydrous ethanol and ultrapure water, and then it was freeze-dried in vacuum overnight, and vacuum-dried to obtain the MCM-41 type MSN.

100 mg of dried sample MSN was weighed and dispersed in a beaker containing 80 mLDMSO. To an EP tube was added 1 mL of DMSO solution containing 1 mg of FA and 1 mL of APTS, and 0.03 mg of N hydroxysuccinimide (NHS) and 0.3 mg of 1-ethyl-(3-dimethylaminopropyl) carbodiimide hydrochloride (EDAC-HCl) were added and stirred for 2 h. Fifteen mL of toluene and the MSN-DMSO solution was added to FA/APTS and the mixture was stirred at room temperature for 20 h. The product was separated by high speed centrifugation, washed twice with toluene and dried under vacuum to give MSN-FA.

20 mg of MSN-FA was weighed with 1 mL of 2% gelatin aqueous solution and gently shaken at 50°C for 6 h. The mixture was then rapidly injected into 8 mL of deionized water at 4°C. After centrifugation/water washing and re-dispersion, 30 μL of 50% glutaraldehyde solution was added to the gelatin solution at a rate of 0.05 mL min-1 to cross-link it. Subsequently, the solution was kept at 40 °C and stirred at 600 rpm for 6 h. Then 20 ng of EDAC·HC1 and 10 mg of NHS dissolved in 500 μL of ultrapure water were dispersed before being added to the nanoparticle mixture, followed by the addition of an aminocarbamoylated PEG (20 mg, ≈4 μmol) solution with a molecular weight of 5 kDa. The mixture was stirred at room temperature for 16 h before centrifugation with ultrapure water and washing to obtain MSN-FA@Gelatin-PEG (PGFMSN) particles.

III. B. Synthesis of PGFMSN particles loaded with adriamycin

Adriamycin hydrochloride (DOX) was used as a model drug for the loading and controlled release behavior of PGFMSN particles evaluated because of its good fluorescence properties and water solubility. DOX-loaded PGFMSN (DOX/PGFMSN) was prepared by mixing 20 mg of MSN-FA with 500 μL of DOX solution at a concentration of 0.01 molL-1 pH 7.2 overnight and then centrifuging to remove the excess DOX. The remaining pellet was gently shaken with 1 mL of 2% gelatin aqueous solution at 50 °C for 6 h, and then the mixture was rapidly injected into 4 °C 8mL deionized water. After two rounds of centrifugation/water washing, 30 μL of 50% glutaraldehyde solution was added to the gelatin solution to cross-link it for 6 h. Gelatin encapsulation and PEG attachment were then achieved as described previously. The amount of pellet encapsulation was obtained by collecting the supernatant and precipitate after centrifugation and measuring the absorbance of UV-visible light at 480 mm, respectively.

III. C. Examination of release curves in culture media

Cells were cultured using no phenol red, containing 5% antibiotics (penicillin, streptomycin), and 10% fetal bovine serum 1640 medium in an incubator containing 5% CO2 at 37°C for 24h before centrifugation, and the supernatant was collected and cryopreserved at -70°C until ready for use. To examine the MMP-2 stimulus response release behavior in media from different cell lines, DOX/PGFMSN samples were placed in a quartz cuvette and 100 μL of cell culture medium was carefully added. Release was examined by detecting particle fluorescence intensity at 560 nm (480 nm excitation) [24]. Two different negative control experiments were also performed: one with medium from the L02 cell line and the other with medium supplemented with MMP-2 inhibitor. All fluorescence values were compared with those of fresh medium.

III. D. Flow cytometry analysis

Quantitative examination of cellular phagocytosis was done by FACScan flow cytometer.T-29 cells were inoculated in 6-well plates containing 10% fetal bovine serum 1640 medium as well as 5×104 cells per well, and incubated in an incubator at 37°C with 5% CO2 for 24 h. DOX (100 μgmL-1), DOX/MSN@Gelatin-PEG were added, DOX/MSN-FA@Gelatin and DOX/PGFMSN pellets to continue incubation for 4 h. The medium was aspirated and washed 3 times with PBS solution. The cells were digested down with a digestion solution of 0.25% trypsin and 0.03% EDTA, and the fluorescence of the extracellular matrix was quenched with Taipan blue (200 μgmL-1). The number of internalized nanoparticles can be obtained by flow cytometry analysis at the FITC-A channel. Cells that were not treated with particles served as controls.

III. E. Examination of anti-tumor effects in vivo

Thymus-free male mice BALB/c were purchased from Shanghai Laboratory Animal Co. Ltd. and cultured under aseptic conditions. All animal operations were performed in strict accordance with the management regulations of the Ministry of Science and Technology for Laboratory Animals of the People's Republic of China. Nude mice 4-6 weeks old, weighing 20-25 g, and injected subcutaneously with 0.2 mL of HT-29 cell suspension solution (2 × 106 cells) in the leg were taken as model mice [25]. When the tumor nodules grew to a volume size of ~100 mm³, 10 well-grown tumor nude mice were randomly assigned into five groups and injected with PGFMSN. DOX (1 mg DOX kg-1), DOX/MSN-FA@Gelatin (1 mg DOX kg-1), DOX/MSN@Gelatin-PEG (1 mg DOX kg-1 and DOX/PGFMSN (1 mg DOX kg-1). Drugs were injected through the tail vein every other day, and tumor length and width were measured with vernier calipers for each nude mouse. Measurements were repeated three times. Tumor volume was calculated using the following equation:

$$\text{Tumor volume} = (\text{tumor length} \times \text{the square of tumor width})/2 \tag{5}$$

The potential toxicity of the drug was also monitored by measuring the body weight of each rat every other day.

IV. 4. Experimental results and analysis

IV. A. Adriamycin preparation and performance evaluation

IV. A. 1) Preparation and characterization of various nanoparticles

(1) FT-IR

The infrared profiles of CS, N-acetylated CS, CS-RAFT reagent and CS-g-PNIPAM polymer are shown in Fig. 2. The absorption peaks at 1086 and 1033 cm-1 can be presumed to be the C3-OH and C6-OH of CS, and it can be clearly seen that the characteristic peak of CS at 1592 cm-1 (-NH2) disappears after the successful synthesis of CS-g-PNIPAM. Comparing with the original CS, the CS-RAFT reagent showed an absorption peak at 1722 cm-1 (C=O),and the absorption peak of the trisulfide unit (1067 cm-1) was not observed due to the strong overlapping absorption of CS between 955 cm-1 and 1200 cm-1. For CS-g-PNIPAM, the presence of PNIPAM was evidenced by the characteristic peaks at 1466 cm-1 (-CH3) and 1644 cm-1 (C=O), and the intensity of the absorption peaks was considerably enhanced in the CS-g-PNIPAM profile. In addition compared to CS, the copolymer showed new absorption peaks at 1395 cm-1 and 1366 cm-1, which proved the presence of isopropyl group in NIPAM, these results further proved the successful synthesis of CS-g-PNIPAM.

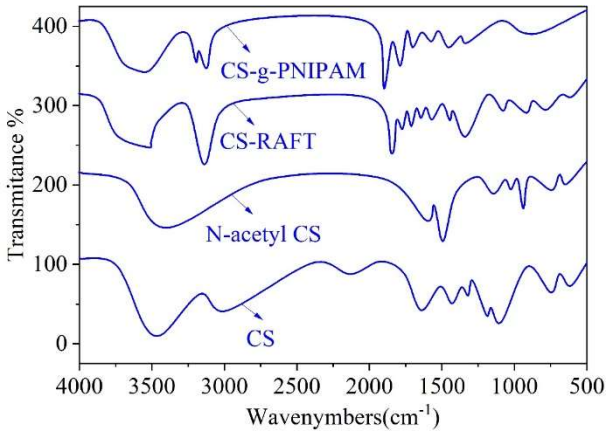

Figure 2: FT-IR spectra of CS, N-acetyl CS, CS-RAFT, and CS-g-PNIPAM

(2) 1H NMR

In addition, we also verified the successful synthesis of NIPAM and L-peptide with CS by 1HNMR.The NMR profile of L-CS-g-PNIPAM nanoparticles is shown in Fig. 3. It is obvious in the figure that the characteristic resonance peaks of PNIPAM are 0.81-2.10 ppm and 7.85 ppm, respectively, indicating that CS-g-PNIPAM was successfully synthesized by using CS-RAFT reagent.It is also important to note that the dodecyl chain of the RAFT reagent overlaps with the characteristic peaks of PNIPAM. Apparently, two peaks at 1.00-2.22 ppm (-CH-CH2), one peak at 3.92 ppm (-NH-CH<), and a strong methyl peak at 1.10 ppm (-NH-CH <) all attest to the presence of NIPAM. To prepare L-peptide functionalized nanoparticles, N-acetyl group was removed from CS-g-PNIPAM by hydrolysis, and then EDC and NHS were used to activate the carboxyl group of L-peptide to form a highly reactive intermediate, which reacted with the amino group of CS to form a stable amide bond to L-CS-g-PNIPAM nanoparticles. 1H NMR spectroscopy also confirmed that the L -CS-g-PNIPAM nanoparticles as the 1H NMR spectrum of L-CS-g-PNIPAM showed new characteristic peaks brought by L-peptide.The absorption peak at 8.69 ppm is a typical characteristic peak of aromatic hydrocarbons in L-peptide, which indicates the successful binding of L-peptide residues to the CS backbone.The absorption peak at 8.69 ppm is a typical peak of aromatic hydrocarbons in L-peptide, which indicates the successful binding of L-peptide residues to the CS backbone.

(3) Physicochemical characteristics of nanoparticles

The physicochemical properties of various nanoparticles are shown in Table 3.Since L-CS-g-PNIPAM copolymers are prone to self-assembly in aqueous solution to encapsulate insoluble drugs, PTX can act through physical hydrophobicity to the hydrophobic center of L-CS-g-PNIPAM nanoparticles. The nanomaterials self-assembled into core-shell nanostructures in aqueous solution at room temperature and neutral pH (7.4), and the water-insoluble and pH-sensitive CS fragment as a core structure could be structurally collapsed in acidic environment, and the water-soluble PNIPAM formed an external shell structure. High-performance liquid chromatography (HOLC) analysis showed that the nanoparticles had a DL of 13.6% and an EE of 75.2%, indicating that the L-CS-g-PNIPAM nanoparticles had relatively high EE and DL, which were suitable for the delivery of antitumor drugs. The nucleation of PTX-encapsulated nanoparticles had an effect on the particle size of the nanoparticles, and the smaller particle size of the PTX-encapsulated nanoparticles compared with the unloaded nanoparticles indicated that the drug

encapsulation enhanced the hydrophobic interaction force between it and the carrier, which resulted in the reduction of the particle size of the nanomaterials. All the prepared nanoparticles had a particle size of less than 350 nm with a more uniform size distribution (PDI < 0.45), which is suitable for targeting tumors by EPR effect, and the size distribution is also suitable for intravenous drug delivery.

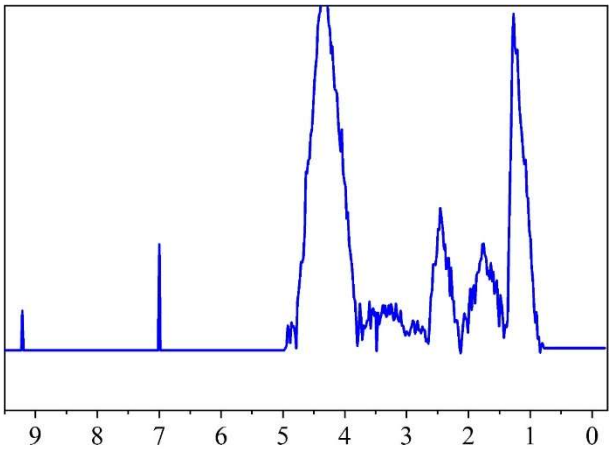

Figure 3: 2-41H NMR spectrum of L-CS-g-PNIPAM NPs

Table 3: The physicochemical properties of various nanoparticles

	Particle size (nm)	Zeta potential (mV)	PDI	DL (%)	EE (%)
CS	204.5±16.4	31.7±2.8	0.331		
N-acetyl CS	226.4±19.9	14.9±2	0.429		
CS-RAFT	252.8±21.2	14.1±2.8	0.304		
CS-g-PNIPAM	267.7±20.5	14.2±2.2	0.35		
L-CS-g-PNIPAM	278.9±25.7	19.2±3.3	0.243		
L-CS-g-PNIPAM-PTX	275.1±19.2	18.8±1.7	0.214	13.6±0.8	75.2±5.2

IV. A. 2) Slow controlled release of PTX

Dialysis method was used to investigate the effect of environmental stimuli on drug release from L-CS-g-PNIPAM-PTX by incubating self-assembled nanoparticles in buffer at different temperatures (37°C,25°C) and different pH (5.0,7.4).The cumulative release rate of PTX at pH=7.4 and 5.0 for three days is shown in Fig. 4.From the L-CS-g-PNIPAM nano drug release it can be seen that PTX release was slow at pH 7.4 and accelerated at decreasing pH. In a simulated neutral pH (7.4) environment, where PTX is encapsulated within an insoluble CS core, it can be observed that the release rate of PTX over 72h is very low. In contrast, under acidic conditions that mimic tumor pH (5.0), the release rate of PTX was significantly higher due to the structural transformation of the core-shell nanocarrier under these conditions, whereas the CS-based copolymer was exposed to acid degradation. After the initial rapid release phase, the release rate was greatly reduced as the release time of PTX was prolonged and the release rate gradually stabilized. This is due to the fact that the CS-g-PNIPAM conjugated chain fragments hidden in the interior are digested by the acid, which gradually exposes the PNIPAM to the surface of the spheres during the acid degradation process due to its immiscibility with the PNIPAM and the continuous movement of the polymer chains. The figure also shows the significant changes in the release of PTX from L-CS-g-PNIPAM nanoparticles at different temperatures. Within 72 h, only 60% PTX was released from L-CS-g-PNIPAM nanoparticles at 25°C, whereas at 37°C, the released PTX increased to 85%. The early and rapid drug release at 25°C and 37°C was attributed to the drug attached on the surface of L-CS-g-PNIPAM nanoparticles. Whereas, the slower rate of PTX release at the later stage at 25°C was due to the stable hydrophilic protection formed by the PNIPAM units on the surface of the nanocarriers. However, when the temperature was increased to 37°C, the increase in the PTX release rate was due to the collapse of the copolymer structure, probably due to the structural alteration of the L-CS-g-PNIPAM nanoparticles caused by the temperature-induced phase transition of PNIPAM. Based on the release profile data, this pH- and temperature-sensitive drug carrier is well suited for application in cancer therapy.

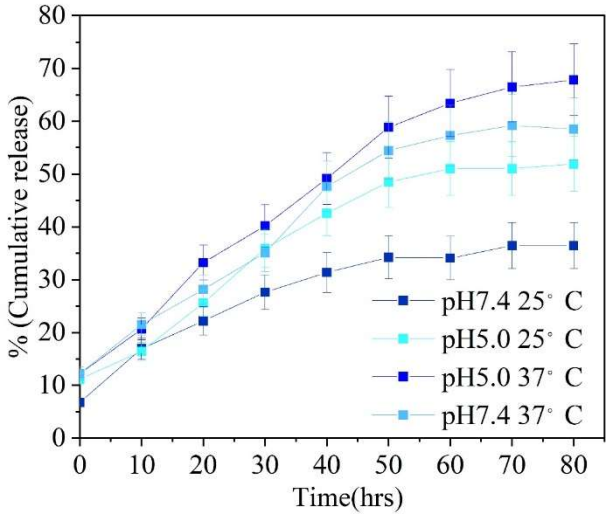

Figure 4: PTX is the cumulative release rate for three days under ph= 7.4 and 5.0

IV. B. Evaluation of the effectiveness of utilization

IV. B. 1) In vivo assessment of anti-tumor effects of nanoparticles

In order to determine the anticancer effects of different treatment strategies, at the end of the experiment, the Cu content in all major organs and tumor tissues of mice in the PBS control group, CuS (+NIR) treatment group and CuS-PEI-siRNA-SFNs (+NIR) treatment group was taken and counted. The biodistribution of Cu in mice in different treatment groups at the 15th day of administration is shown in Figure 5.The Cu content in lung and tumor tissues was significantly higher in both the CuS (+NIR) treatment group and CuS-PEI-siRNA-SFNs (+NIR) treatment group than that in the PBS control group, which provided a good basis for the Cu death of mice in both the CuS (+NIR) treatment group and CuS-PEI-siRNA-SFNs (+NIR) treatment group through Cu death. NIR) treatment group provided evidence for the inhibition of metastatic breast cancer growth through the copper death effect. In addition, the content of Cu in both lung and tumor tissues was significantly higher in the CuS-PEI-siRNA-SFNs (+NIR) treatment group than in the CuS (+NIR) treatment group, which was attributed to the long-lasting slow-release effect of copper ions in CuS-PEI-siRNA-SFNs compared with CuS.

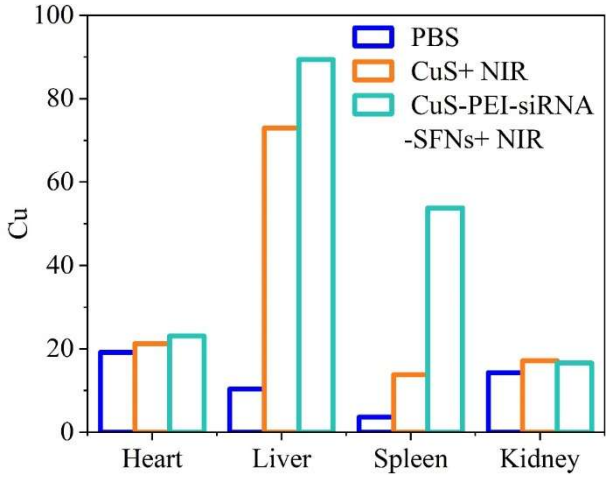

Figure 5: In vivo biodistribution of Cu in different treatment groups

IV. B. 2) Biosafety assessment of nanoparticles

Biosafety is a key issue for nanomedicines in cancer therapy. Firstly, in vitro hemolysis experiments were performed, and the results showed that CuS showed significant hemolysis in the presence of 100 μg/mL Cu, with a hemolysis rate of 49.2%, implying that serious hemolytic toxicity may occur if CuS is used in clinical therapy. In contrast, the hemolysis rate of CuS-PEI-siRNA-SFNs in the presence of an equal amount of Cu (100 μg/mL) was only negligible at 0.1%. The hemolysis rate of CuS-PEI-siRNA-SFNs was still significantly lower than that of CuS in the presence of an equal amount of Cu (200-300 μg/mL).These indicate that CuS-PEI-siRNA-SFNs have superior blood

compatibility than CuS.The hemolysis experiments of PBS, CuS, CuS-PEI-siRNA-SFNs and TritonX-100 were shown in Figure 6. 100 hemolysis experiments are shown in Figure 6 (Figures a~b denote the hemolysis experiments of PBS, CuS, CuS-PEI-siRNA-SFNs and TritonX-100, respectively).

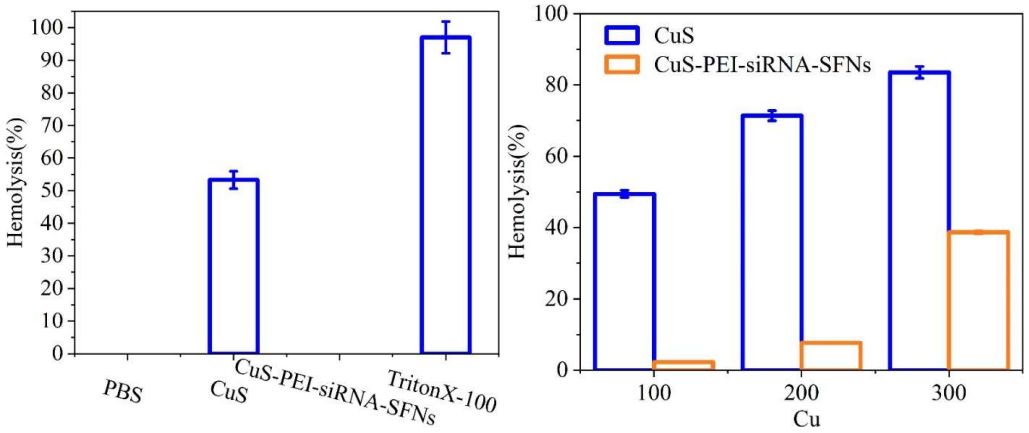

(a) Hemylous experiment of PBS, CuS, CuS-PEI-siRNA-SFNs

(b) Tritonx-100 hemolysis experiment

Figure 6: Hemolysis test of PBS, CuS, CuS-PEI-siRNA-SFNs and TritonX-100

The liver and kidney function analysis of mice in different treatment groups at the end of the experiment is shown in Fig. 7 (a~d denote the groups of alanine aminotransferase (ALT), aspartate aminotransferase (AST), creatinine (CREA), and urea nitrogen (UREA), respectively). The blood biochemical indices were further tested to show that there was no significant difference between the four indices of liver and kidney function, including alanine aminotransferase (ALT), aspartate aminotransferase (AST), creatinine (CREA), and urea nitrogen (UREA) in each of the different treatment groups. And these liver and kidney biochemical indexes were within normal values.

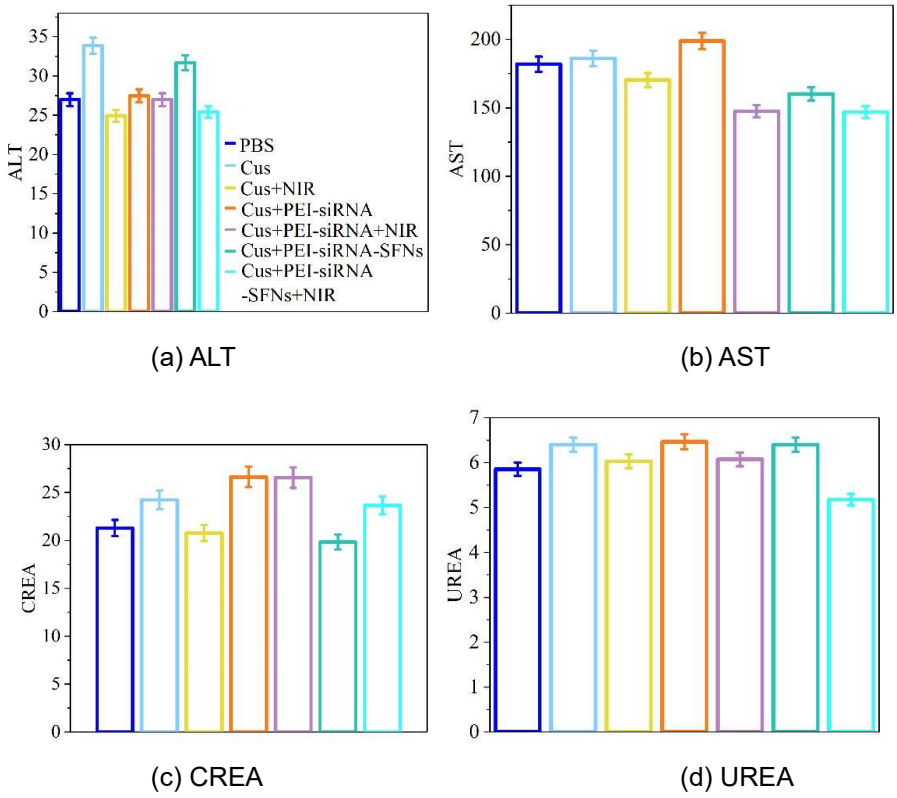

(a) ALT

(b) AST

(c) CREA

(d) UREA

Figure 7: Hepatic and renal functions analysis of mice in various treatment groups

V. Conclusion

In this study, two drug-carrying systems were successfully constructed: nanoparticles based on L-CS-g-PNIPAM and a photothermal slow-release system based on CuS-PEI-siRNA-SFNs, and the successful preparation of the nanocarriers and their superior performance as adriamycin carriers were confirmed by various characterization means.FT-IR and 1H NMR analyses confirmed the The successful synthesis of L-CS-g-PNIPAM, its characteristic peaks at 1466 cm-1 (-CH3) and 1644 cm-1 (C=O) as well as the aromatic hydrocarbon characteristic peak of L-peptide at 8.69 ppm clearly showed the introduction of the modifying groups. Physicochemical characterization showed that the L-CS-g-PNIPAM-PTX nanoparticles with a particle size of 275.1±19.2 nm and a zeta potential of 18.8±1.7 mV exhibited good dispersion stability (PDI=0.214). The carrier exhibited remarkable pH and temperature responsiveness, with significantly higher drug release efficiency at pH 5.0 and 37°C, and a cumulative release rate of up to 85% within 72 hours, compared with only 60% under normal physiological conditions (pH 7.4, 25°C), demonstrating its excellent tumor microenvironment responsiveness. Biosafety evaluation showed that CuS-PEI-siRNA-SFNs exhibited a very low hemolysis rate (0.1%), which was much better than that of bare CuS nanoparticles (49.2%). The in vivo distribution study further confirmed that the copper content in lung and tumor tissues was significantly higher in the CuS group than in the CuS group and the control group in the CuS group, suggesting that the system has better targeting and long-lasting slow-release ability. Meanwhile, the results of liver and kidney function indexes (ALT, AST, CREA, UREA) showed that there was no significant difference between the treatment groups and they were all within the normal range, which confirmed the safety of the nanocarrier system. In conclusion, the photothermal slow-release nanocarrier system of adriamycin designed in this study has ideal drug slow-release performance, good biological safety and excellent antitumor effect, which provides a new idea for anticancer drug delivery and tumor therapy.

Funding

This work was supported by Major Project of Henan Province Higher Education Teaching Reform Research and Practice Project for the year 2024 (Project Number: 2024SJGLX0634).

References

[1] Akash, S. (2021). An Overview of advanced treatment of Cancer Where are we today?. International Journal of Multidisciplinary Research and Explorer, 1(3), 20-25.

[2] Fidler, M. M., Bray, F., & Soerjomataram, I. (2018). The global cancer burden and human development: A review. Scandinavian journal of public health, 46(1), 27-36.

[3] Sritharan, S., & Sivalingam, N. (2021). A comprehensive review on time-tested anticancer drug doxorubicin. Life sciences, 278, 119527.

[4] Sheibani, M., Azizi, Y., Shayan, M., Nezamoleslami, S., Eslami, F., Farjoo, M. H., & Dehpour, A. R. (2022). Doxorubicin-induced cardiotoxicity: an overview on pre-clinical therapeutic approaches. Cardiovascular Toxicology, 22(4), 292-310.

[5] Mohamed, N., Hashad, M., Amein, K., & Hafez, E. (2018). Genotoxic Effects of the Anti-Cancer Drug Doxorubicin (Dxr) in the Bone Marrow Cells of Swiss Albino Mice (Mus musculus). Journal of Agricultural Chemistry and Biotechnology, 9(9), 211-215.

[6] Haftcheshmeh, S. M., Jaafari, M. R., Mashreghi, M., Mehrabian, A., Alavizadeh, S. H., Zamani, P., ... & Gheybi, F. (2021). Liposomal doxorubicin targeting mitochondria: A novel formulation to enhance anti-tumor effects of Doxil® in vitro and in vivo. Journal of Drug Delivery Science and Technology, 62, 102351.

[7] Ibrahim, M., Abuwatfa, W. H., Awad, N. S., Sabouni, R., & Husseini, G. A. (2022). Encapsulation, release, and cytotoxicity of doxorubicin loaded in liposomes, micelles, and metal-organic frameworks: a review. Pharmaceutics, 14(2), 254.

[8] Islam, M. R., Patel, J., Back, P. I., Shmeeda, H., Adamsky, K., Yang, H., ... & La-Beck, N. M. (2022). Comparative effects of free doxorubicin, liposome encapsulated doxorubicin and liposome co-encapsulated alendronate and doxorubicin (PLAD) on the tumor immunologic milieu in a mouse fibrosarcoma model. Nanotheranostics, 6(4), 451.

[9] Nishimoto, A. (2022). Effective combinations of anti-cancer and targeted drugs for pancreatic cancer treatment. World Journal of Gastroenterology, 28(28), 3637.

[10] Iijima, Y., Bandow, K., Sano, M., Hino, S., Kaneko, T., Horie, N., & Sakagami, H. (2019). In vitro assessment of antitumor potential and combination effect of classical and molecular-targeted anticancer drugs. Anticancer Research, 39(12), 6673-6684.

[11] Kydd, J., Jadia, R., Velpurisiva, P., Gad, A., Paliwal, S., & Rai, P. (2017). Targeting strategies for the combination treatment of cancer using drug delivery systems. Pharmaceutics, 9(4), 46.

[12] Pushpalatha, R., Selvamuthukumar, S., & Kilimozhi, D. (2017). Nanocarrier mediated combination drug delivery for chemotherapy–A review. Journal of drug delivery science and technology, 39, 362-371.

[13] Beniwal, N., Verma, A., Putta, C. L., & Rengan, A. K. (2024). Recent trends in bio-nanomaterials and non-invasive combinatorial approaches of photothermal therapy against cancer. Nanotheranostics, 8(2), 219.

[14] Li, C., Cheng, Y., Li, D., An, Q., Zhang, W., Zhang, Y., & Fu, Y. (2022). Antitumor applications of photothermal agents and photothermal synergistic therapies. International Journal of Molecular Sciences, 23(14), 7909.

[15] Ge, R. L., Yan, P. N., Liu, Y., Li, Z. S., Shen, S. Q., & Yu, Y. (2023). Recent advances and clinical potential of near infrared photothermal conversion materials for photothermal hepatocellular carcinoma therapy. Advanced Functional Materials, 33(29), 2301138.

[16] Karthikeyan, L., & Vivek, R. (2022). Synergistic anti-cancer effects of NIR-light responsive nanotherapeutics for chemo-photothermal therapy and photothermal immunotherapy: A combined therapeutic approach. Advances in Cancer Biology-Metastasis, 4, 100044.

[17] Nam, J., Son, S., Ochyl, L. J., Kuai, R., Schwendeman, A., & Moon, J. J. (2018). Chemo-photothermal therapy combination elicits anti-tumor immunity against advanced metastatic cancer. Nature communications, 9(1), 1074.

[18] Ye, L., Chen, Y., Mao, J., Lei, X., Yang, Q., & Cui, C. (2021). Dendrimer-modified gold nanorods as a platform for combinational gene therapy and photothermal therapy of tumors. Journal of Experimental & Clinical Cancer Research, 40, 1-16.
[19] Habiburrahman, M., Putra, A. B., & Rakasiwi, M. I. D. (2023). Combining Photothermal Therapy with A Nanohybrid-Based Drug Delivery Strategy for Slow-Released Doxorubicin: A Treatment for Hepatocellular Carcinoma. Indonesian Journal of Cancer, 17(2), 167-175.
[20] Wang, X., Ma, Y., Chen, H., Wu, X., Qian, H., Yang, X., & Zha, Z. (2017). Novel doxorubicin loaded PEGylated cuprous telluride nanocrystals for combined photothermal-chemo cancer treatment. Colloids and Surfaces B: Biointerfaces, 152, 449-458.
[21] Liang, J., Liu, J., Jin, X., Yao, S., Chen, B., Huang, Q., ... & Wang, B. (2020). Versatile nanoplatform loaded with doxorubicin and graphene quantum dots/methylene blue for drug delivery and chemophotothermal/photodynamic synergetic cancer therapy. ACS Applied Bio Materials, 3(10), 7122-7132.
[22] Junhui Ma,Nan Ma,Yan Tang,Meiyu Shao,Lei Wang,Jun Liu & Wei Zhang. (2025). A facile and universal coating Orn-Val-OH for enhancing surface biocompatibility of biomedical material. Applied Surface Science,700,163241-163241.
[23] Dina A. Eltahan,Rania K. Eid,Shimaa M. Ashmawy & Gamal M. El Maghraby. (2025). Nanoemulsion for enhanced absorption and anti-tumor activity of dasatinib. Journal of Drug Delivery Science and Technology,107,106870-106870.
[24] Wenjing Jiang,Qiuli Wang,Xiaoyan Zhang,Husheng Yang & Xinggang Yang. (2025). Semaglutide sustained-release microspheres with single-phase zero-order release behavior: Effects of polymer blending and surfactants. Journal of Drug Delivery Science and Technology,107,106793-106793.
[25] Shuxin Song,Jingbo Wang,Xiaohu Ouyang,Renyin Huang,Fang Wang,Junke Xie... & Desheng Hu. (2025). Therapeutic connections between pyroptosis and paclitaxel in anti-tumor effects: an updated review..Naunyn-Schmiedeberg's archives of pharmacology,(prepublish),1-17.